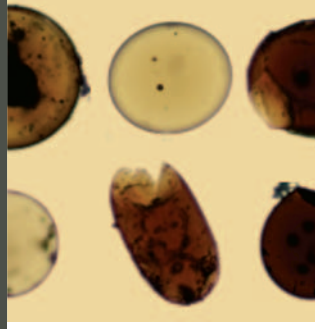

High-Spatial-Resolution Geochronology

Alexander A. Nemchin[1], Matthew S. A. Horstwood[2], and Martin J. Whitehouse[3]

1811-5209/13/0009-0031$2.50 DOI: 10.2113/gselements.9.1.31

High-spatial-resolution isotope analyses have revolutionised U–(Th–)Pb geochronology. These analyses can be done at scales of a few tens of microns or less using secondary ion mass spectrometry or laser ablation inductively coupled plasma mass spectrometry. They allow determination of the internal age variation of uranium- and thorium-bearing minerals and as a consequence much greater understanding of Earth system processes. The determination of variation on the micron scale necessitates the sampling of small volumes, which restricts the achievable precision but allows discrimination of discrete change, linkage to textural information, and determination of multiple isotopic and elemental data sets on effectively the same material. High-spatial-resolution analysis is being used in an increasing number of applications. Some of these applications have become fundamental to their scientific fields, while others have opened new opportunities for research.

KEYWORDS: high-spatial-resolution analyses, isotopes, zircon, mineral zoning, sedimentary provenance

INTRODUCTION

Modern geochronology has evolved by gradual sample-size reduction, decreasing from the analysis of whole-rock and multigrain fractions to single mineral grains and grain fragments. These advances have culminated in modern high-spatial-resolution methods that can determine isotope ratios from within single zones of crystals as small as 1–5 microns across. A complete history of this transformation and a listing of the full range of achievements of these methods are beyond the scope of this article (a comprehensive summary is given by Davis et al. 2003). Instead we focus on the fundamental capabilities that give high-spatial-resolution methods their unique niche in geochronology.

Analysis using secondary ion mass spectrometry (SIMS) and laser ablation inductively coupled plasma mass spectrometry (LA–ICP–MS) requires comparison of measured values from a sample with those from a reference material whose ratios have been previously calibrated (typically by isotope dilution thermal ionisation mass spectrometry; ID-TIMS). Because the efficiency of this calibration varies among media for the same elemental species, matrix-matched calibration is usually essential. As a consequence, the precision and accuracy of analyses of elemental ratios in unknown samples is limited by the precision and accuracy of analyses of these ratios in the reference (commonly natural) materials. However, the inherent lack of chemical preparation when using SIMS and LA–ICP–MS techniques allows microstructural and chemical zonation in minerals and rocks to be targeted directly, rapidly and relatively easily at a precision level (usually not better than 2%, 2σ) still appropriate for answering a multitude of geochronology questions that would otherwise be difficult or impossible to address by lower-spatial-resolution, higher-precision geochronological methods.

More than two decades of extensive application of high-spatial-resolution techniques have highlighted areas where these methods are uniquely suited to solving geochronological problems. This article highlights applications that illustrate the state of the art and the need for high-spatial-resolution geochronology in the geochronologist's toolkit; we particularly focus on some less well-known studies that illustrate new directions for future research. The examples given here concentrate on U–Th–Pb age determinations, but there are many examples of the utility of high-spatial-resolution analysis in other geochronometric systems, particularly $^{40}Ar/^{39}Ar$ (see Hodges et al. 2005 for a review).

GEOCHRONOLOGICAL APPLICATIONS OF HIGH-SPATIAL-RESOLUTION METHODS

Intragrain and In Situ Studies

A unique niche for high-spatial-resolution techniques in geochronology (and geochemistry in general) is provided by the small, often submicron-scale complexities of the analysed materials. Rock-forming and accessory minerals typically display zoning in their elemental and isotopic compositions, including variations in age of minerals used as geochronometers. This zoning may reflect the incorporation of material older than the main age of the crystal ("inheritance"), result from chemical evolution of the magma or fluid from which these minerals crystallised or were precipitated, or arise from post-crystallisation processes that have reequilibrated and/or disturbed the mineral. This zonation can be revealed and "mapped" at the micron scale through the use of optical microscopy and/or elemental quantification techniques (cathodoluminescence or backscattered electron imaging and

1 Department of Applied Geology, Curtin University
PO Box U1987, Perth, WA 6845, Australia
E-mail: A.Nemchin@curtin.edu.au

2 NERC Isotope Geosciences Laboratory
British Geological Survey, Keyworth, NG12 5GG, UK
E-mail: msah@bgs.ac.uk

3 Swedish Museum of Natural History
Box 50007, SE104 05 Stockholm, Sweden

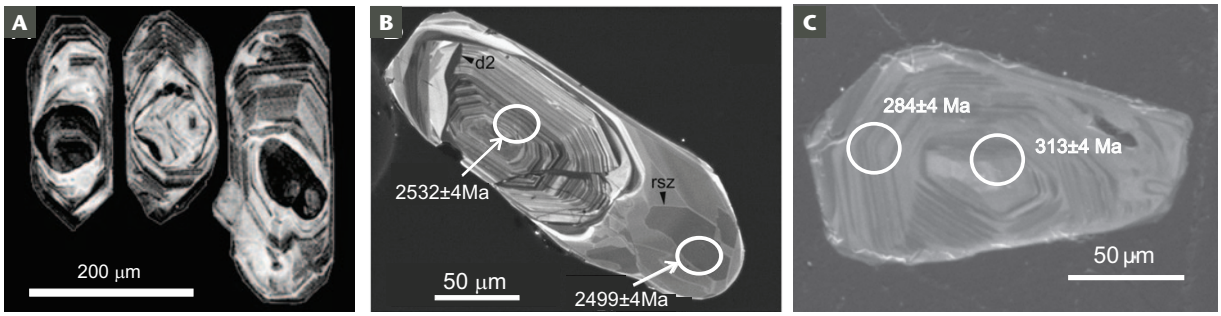

Figure 1 Zircon grains showing different types of internal complexity. (**A**) Cores with ages older than 440 Ma, overgrown by magmatic rims defining the crystallisation time of the Why Worry Tonalite in southeastern Australia as 393 ± 2.6 Ma (Kemp et al. 2005). Image reproduced with permission from Springer (**B**) Magmatic core overgrown by a metamorphic rim in zircon from the Xianjinchang tonalite, Eastern Block of the North China Craton (Grant et al. 2009). Image reproduced with permission from Elsevier (**C**) Igneous core overgrown by an igneous rim in zircon from granite formed as a result of Paleozoic felsic magmatism during the Terra Australis accretionary orogeny; similar internal structures in the core and rim require high-spatial-resolution analyses of both parts of the grain to recognise that the zircon is inhomogeneous (Cawood et al. 2011). Uncertainties of individual analyses in (B) and (C) are 1σ.

electron microprobe). High-spatial-resolution geochronological techniques, with their typical 5–40 micron spatial resolution, are therefore required to determine the age of individual parts of zoned crystals, and the combination of image analysis with the geochronology of mineral grains is essential for improving the interpretation of geochronology data.

Both SIMS and LA–ICP–MS techniques involve the analysis of polished or sectioned samples, which allows U–Pb ages to be linked to (1) microstructures commonly observed in these minerals, likely reflecting complexity of their history, and (2) textures of the host rocks when U–Pb analyses are done in situ using thin sections or polished rock chips. The most common use of microprobe techniques is the U–Pb geochronology of zircon, where the isotopic analysis of small spots within each grain combined with the investigation of internal structures of these grains allows the determination of chronological information from structurally complex zircon grains recording multiple crystallisation and/or recrystallization events (Scherer et al. 2007). Numerous published cases illustrate how these techniques permit us to distinguish between the magmatic parts of zircon grains and inherited cores (Fig. 1A), recognise metamorphic overgrowths (Fig. 1B), or just allow us to avoid submicron-scale complexities in the grains. While some complex internal relationships in zircon grains are easily recognisable from the images alone, the identification of others, where grains record multiple metamorphic episodes or where igneous cores are overgrown by magmatic rims (Fig. 1C), requires a combined application of imaging and SIMS or LA–ICP–MS techniques. Consequently, combining imaging techniques and high-spatial-resolution chronological methods is essential for accurate timing of rocks with a complex history.

A comparatively underutilised but powerful tool for studying zoned age patterns in geochronometric minerals is scanning ion imaging using SIMS (Fig. 2). In this method, the primary ion beam is rastered at high frequency over a large sample area (e.g. 100 × 100 microns), while the secondary ion beam is measured in low-noise ion-counting detectors. Coupling the primary-beam raster and the secondary-beam realignment deflectors allows the mass spectrometer to perform the high-mass-resolution measurements necessary for Pb isotopes. The ion image is generated by software that links a specific ion count to a given pixel in the raster; in practice, images are accumulated over many cycles in order to yield reasonable integrated intensities and low counting-statistic uncertainties. The spatial resolution of the image is determined solely by the primary-beam spot size and is typically as low as just a few microns. In geochronological applications, this method can be used to generate $^{207}Pb/^{206}Pb$ age maps of zircon that can reveal processes of isotopic redistribution within a crystal (Fig. 2). In this example, heterogeneity in apparent age is an artefact of ultrahigh-temperature metamorphism, illustrating how mapping methods can be used to test the

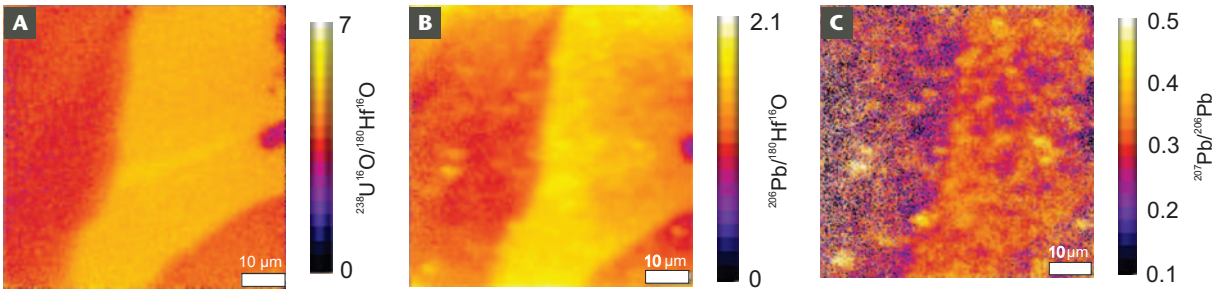

Figure 2 SIMS ion images of an area within a zircon grain from an orthogneiss (Napier Complex, Antarctica), modified after Kusiak et al. (2013). (**A**) The ^{238}U relative (i.e. normalised to the $^{180}Hf^{16}O$ peak) intensity reflects variations in U concentrations, which determine the zircon zoning pattern. (**B**) The ^{206}Pb relative intensity defines the variability of ^{206}Pb, which in general follows the U distribution. However, the image also shows a number of <2–3 micron-size "hot" spots with significant amounts of Pb. This increase in Pb concentration does not reflect a similar increase in U content (image A), suggesting that the radiogenic Pb in the "hot" spots is not supported by U. This produces a sharp variation in $^{207}Pb/^{206}Pb$ and apparent age (**C**), with some spots indicating apparent ages in excess of 4.0 Ga (bright yellow) while some are as young as 2.5 Ga (purple). Although the apparent-age map uses $^{207}Pb/^{206}Pb$ uncorrected for common Pb, ^{204}Pb measured simultaneously is insignificant and does not contribute to the observed heterogeneity in the $^{207}Pb/^{206}Pb$ ratio.

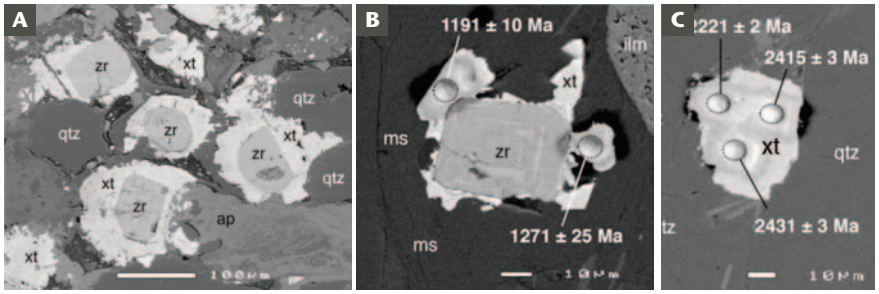

Figure 3 Xenotime growth structures imaged using a backscattered electron detector. Zr = zircon, xt = xenotime, qtz = quartz, ilm = ilmenite, ms = muscovite, ap = apatite. Oval pits in B and C are SIMS analytical areas, and Pb–Pb ages (±1σ) are shown. Images from Rasmussen et al. (2011a), reproduced with permission from Springer

veracity of spot ages (Kusiak et al. 2013). The application of mapping discrete domains in minerals and indeed whole-rock materials is a rapidly expanding area of research likely to contribute significantly to high-spatial-resolution geochronology in the coming decade.

Over the past thirty years, in situ geochronological studies have largely been dominated by SIMS and subsequently LA–ICP–MS U–Pb analysis of zircon. In the last decade, however, other U-bearing minerals, in particular monazite and xenotime, have received increasing attention. These minerals are especially important for dating diagenesis and thereby constraining the depositional age of sediments. Rasmussen et al. (2011a) illustrate complex zircon–xenotime overgrowth textures in sandstones, phyllites and pelitic schists targeted by SIMS using a 5-micron analysis spot. The technique allowed them to discriminate multiple age domains within the xenotime overgrowths indicating the gradual replacement of detrital and diagenetic xenotime by metamorphic xenotime during prograde metamorphism (Fig. 3).

Analysis of Rare Materials

The low sample consumption of high-spatial-resolution geochronological techniques, particularly SIMS, is essential when dealing with unique samples, allowing repeated analysis of effectively the same material in the course of different elemental and isotope investigations. Equally, problem areas within samples (e.g. fractures, inclusions and crystallographic imperfections) can be avoided, based on prior or real-time imaging techniques, to analyse the best-preserved, most analytically favourable material. Perhaps one of the best examples of this concept is provided by the fast-expanding field of lunar U–Pb geochronology, which now encompasses investigation of a variety of U-bearing minerals including zircon, apatite, baddeleyite, zirconolite and tranquillityite. The physical separation of these minerals from lunar materials would result in substantial sample loss and potential breaking of U-bearing minerals along the multiple fractures existing in lunar samples as a result of their prolonged impact history. By contrast, in situ analysis allows the utilisation of the wealth of textural information available, essential for the interpretation of chronological results in samples that represent a complex mixture of materials originating from different sources. In studies of lunar zircon, this textural information permits the identification and dating of specific groups of igneous rocks, ranging from troctolites and norites to anorthosites and felsites, and now preserved as small submillimetre-size lithic clasts in the lunar impact breccias (Fig. 4a). Textural characterisation also allows recognition of specific types of zircon grains growing in the impact melts and therefore direct dating of the impacts that formed these melts (Fig. 4b). Finally, in situ zircon geochronology combined with the imaging of analysed grains helps to identify complexities inside some zircon grains, giving an opportunity to determine the time of both magmatic crystallisation and the impacts that modified these zircon grains (Fig. 4c, d). To date, the two most significant outcomes of this approach in lunar geochronology have been to establish a minimum age for the crystallisation of the Lunar Magma Ocean at 4417 ± 6 Ma (Nemchin et al. 2009) and to identify a number of large impacts on the Moon significantly predating the Late Heavy Bombardment at about 3.9 Ga (e.g. Grange et al. 2013); the latter event is believed to be responsible for substantial changes in the evolution of planets in the inner Solar System, including Earth.

The analysis of small sample volumes results in lower-precision data, but in some circumstances this compromise is required to arrive at a correct age determination. An example is the case of the multiple analyses of high-Ti volcanic-glass beads extracted from an Apollo 17 soil sample (Fig. 5). Several attempts to analyse lunar volcanic-glass beads using ID-TIMS in the 1970s and 1980s (Tatsumoto et al. 1987) were hindered by terrestrial contamination superimposed on the lunar initial Pb, probably associated with the outer coatings of the glass beads. This resulted in extremely imprecise ages. Mounting these beads for ion

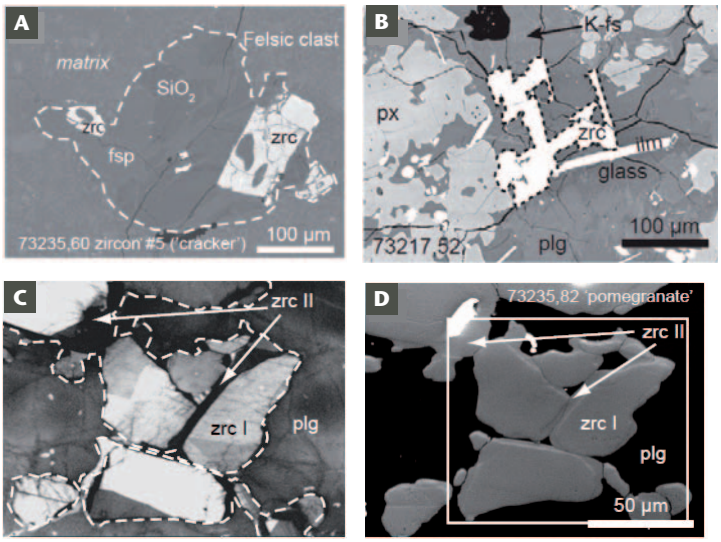

Figure 4 Zircon grains in thin sections of lunar breccia samples showing different textural and microstructural characteristics indicative of their origin and essential for the interpretation of their ages (Grange et al. 2013). (**A**) Backscattered electron (BSE) image of zircon inside a felsic clast (outlined) in Apollo 17 breccia sample 73235 (the age of this grain defines the timing of crystallisation of the igneous host). (**B**) BSE image of zircon in Apollo 17 sample 73217; the zircon grew in a felsic impact melt and allowed dating the impact that formed this melt. (**C**) Cathodoluminescence (CL) image of zircon from an anorthosite clast in Apollo 17 breccia sample 73235 showing crystalline zircon fragments (zrc 1) used to define the time of anorthosite crystallisation. The crystalline fragments are surrounded by amorphous zircon (zrc II) formed as a result of impact and dating this impact. (**D**) BSE image of the same area as (C) demonstrating that the amorphous parts (black in CL) show BSE contrast similar to that of crystalline zircon fragments, which indicates that the amorphous parts preserve zircon's chemical composition. Zrc = zircon, fsp = feldspar, plg = plagioclase, K-fs = K-feldspar, px = pyroxene. Images reproduced with permission from Elsevier

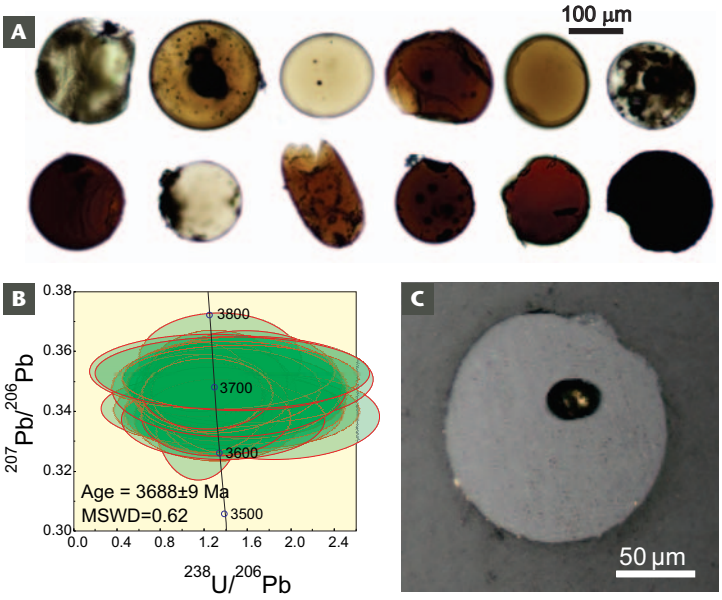

Figure 5 (**A**) Optical images of volcanic-glass beads from the Apollo 17 soil sample. The formation of these beads is linked to eruptions during which magma was thrown into space and broken into small droplets, which solidified and accumulated in the lunar soils. (**B**) Tera-Wasserburg concordia diagram showing SIMS U–Pb analyses of Apollo 17 high-Ti volcanic-glass beads (uncertainties of individual analyses are shown as 2σ). (**C**) BSE image of one of the analysed glass beads showing a SIMS analytical spot. MSWD = mean square of weighted deviates

probe analysis followed by polishing to expose the inner parts of the beads (and cleaning of the mount surface) minimised contamination and allowed the determination of the purely radiogenic Pb component preserved in the beads. Even though both U and Pb concentrations in these glasses are only a few hundred parts per billion, multiple analyses of the 40 beads resulted in a precision equal to 9 Ma (or about 0.2%), assuming that the data contain only analytical scatter and represent a single population.

In this example, the limitations of Pb isotope analysis by SIMS preclude verification of potential heterogeneities below the typical few per cent uncertainties associated with individual spot analyses; however, other methods of discrimination, such as employing chemistry to indicate internal homogeneity of the analysed group of glasses, have already been used to strengthen confidence in the assumption that all the beads belong to the same age population.

Combining Geochronology with Petrogenetic Indicators

The relatively non-destructive nature of high-spatial-resolution analyses allows the determination of ages and the investigation of chemical and isotopic compositions of several elements and isotope systems in the same mineral grain. One of the most studied cases illustrating this capability is the Jack Hills (Australia) detrital-zircon population, which contains the oldest terrestrial grains. This example is a testament to the power of high-spatial-resolution methods, even though the interpretation of the results obtained on these zircon grains remains highly controversial. SIMS U–Pb geochronological studies revealed that the zircon population in the original location described by Compston and Pidgeon (1986) contains ca. 10% of grains that are older than 3.9 Ga (Fig. 6A). The remaining part of the population is dominated by zircon grains with ages between 3.4 and 3.2 Ga, with the youngest recorded ages being about 3.0 Ga (e.g. Pidgeon and Nemchin 2006). Heavy oxygen isotope compositions observed in some >3.9 Ga zircon grains (Fig. 6B) have been used to suggest a supracrustal component in the source of melts from which these grains crystallised, as well as the presence of surface water (Cavosie et al. 2005). Elevated and normal light rare earth element concentrations (Peck et al. 2001) reflect variable alteration in some grains (Fig. 6C) (Cavosie et al. 2006). A felsic source for >3.9 Ga Jack Hills zircon grains was proposed from the crystallisation-temperature estimates for these zircon grains, which range between about 650 °C and 750 °C based on their Ti content (Watson and Harrison 2005) as well as on the presence of inclusions dominated by quartz, K-feldspar, micas and monazite (Hopkins et al. 2010). Results from combined SIMS U–Pb and LA–ICP–MS

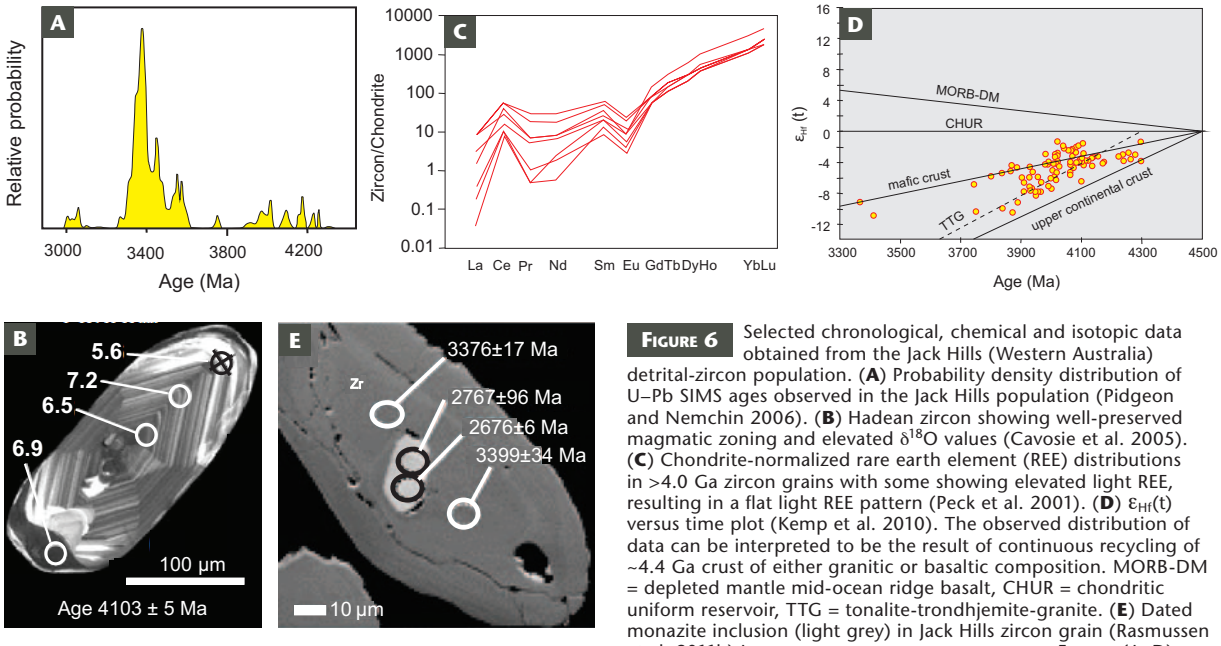

Figure 6 Selected chronological, chemical and isotopic data obtained from the Jack Hills (Western Australia) detrital-zircon population. (**A**) Probability density distribution of U–Pb SIMS ages observed in the Jack Hills population (Pidgeon and Nemchin 2006). (**B**) Hadean zircon showing well-preserved magmatic zoning and elevated $\delta^{18}O$ values (Cavosie et al. 2005). (**C**) Chondrite-normalized rare earth element (REE) distributions in >4.0 Ga zircon grains with some showing elevated light REE, resulting in a flat light REE pattern (Peck et al. 2001). (**D**) $\varepsilon_{Hf}(t)$ versus time plot (Kemp et al. 2010). The observed distribution of data can be interpreted to be the result of continuous recycling of ~4.4 Ga crust of either granitic or basaltic composition. MORB-DM = depleted mantle mid-ocean ridge basalt, CHUR = chondritic uniform reservoir, TTG = tonalite-trondhjemite-granite. (**E**) Dated monazite inclusion (light grey) in Jack Hills zircon grain (Rasmussen et al. 2011b) Images reproduced with permission from Elsevier (A–D) and Geological Society of America publications (E)

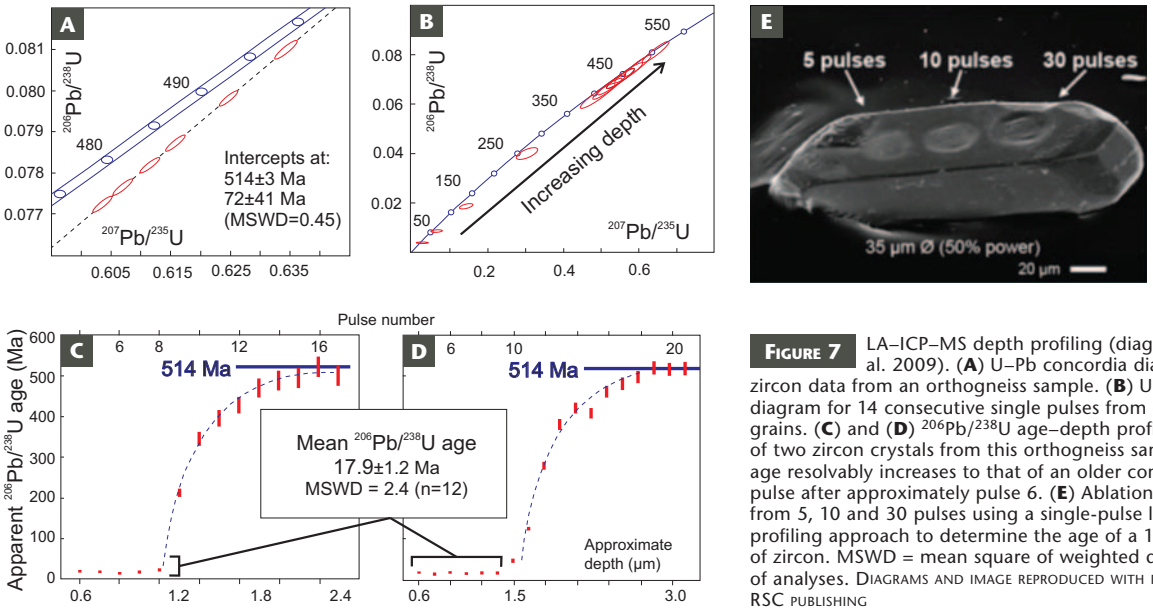

Figure 7 LA–ICP–MS depth profiling (diagrams from Cottle et al. 2009). (**A**) U–Pb concordia diagram using ID-TIMS zircon data from an orthogneiss sample. (**B**) U–Pb concordia diagram for 14 consecutive single pulses from one of the analysed grains. (**C**) and (**D**) $^{206}Pb/^{238}U$ age–depth profiles through the rims of two zircon crystals from this orthogneiss sample. Note how the age resolvably increases to that of an older component with each pulse after approximately pulse 6. (**E**) Ablation craters resulting from 5, 10 and 30 pulses using a single-pulse laser ablation depth-profiling approach to determine the age of a 1 µm thick rim phase of zircon. MSWD = mean square of weighted deviates, n = number of analyses. Diagrams and image reproduced with permission from RSC publishing

Hf isotope studies of zircon have also been interpreted to reflect the presence of relatively felsic crust that did not experience any juvenile addition since its formation at about 4.4 Ga (Harrison et al. 2008).

An alternative explanation for the chemical and isotopic features of Jack Hills zircon suggests that these data indicate conditions different from those prevailing on the modern Earth. In particular, heavy oxygen isotope compositions identified in some zircon grains could indicate interaction of basaltic crust with a CO_2-rich atmosphere (Kramers 2007). Hf isotope data (Fig. 6D) are also consistent with a protracted reworking of basaltic crust (Kemp et al. 2010). Furthermore, in a study of inclusions of monazite (Fig. 6E) and xenotime in Jack Hills zircon grains, Rasmussen et al. (2011b) concluded that perhaps all inclusions were formed or profoundly modified by metamorphic events at either 2.68 or 0.8 Ga. Regardless of the differing views and interpretations of information obtained from the studies of Jack Hills zircon, high-spatial-resolution methods have been instrumental in delineating the currently existing controversy and will help to resolve it in the future.

Depth Profiling

Microprobe techniques such as SIMS and LA–ICP–MS are uniquely suited to depth-profiling studies and the determination of isotopic and elemental change on the submicron scale. SIMS U–Pb analysis usually sputters a crater 1–2 microns deep, while a typical laser ablation U–Pb analysis ablates to 15–40 microns depth. However, data obtained using either method can yield time- and hence depth-resolved variation of age and chemistry on the 100-nanometer scale. Depth profiling in geochronology has traditionally been the domain of SIMS techniques (Breeding et al. 2004) but more recently laser ablation has also demonstrated comparable capability.

Using LA–ICP–MS, Cottle et al. (2009) demonstrated the utility of depth profiling in U–Th–Pb geochronology. In their study, single pulses from a laser ablation system coupled to a multicollector ICP–MS apparatus were used to ablate through the crystal face of a zircon thought to possess a thin phase of growth around the edge of the grain. Previous ID-TIMS determinations of single grains had demonstrated a mixing relationship between an older ~514 Ma age component and a younger possibly non-zero age domain, but had not been able to resolve either end-member (Fig. 7A). Although this rim phase was too thin to target using the normal approach of single-spot static ablation on an equatorial section through the zircon grain, depth profiling was successfully used to determine an 18 Ma age for a ~1-micron-thick rim on two different zircon grains; the analysis progressed into the zircon sample in 150-nanometre increments on a pulse-by-pulse basis (Fig. 7B–D). Fig. 7E illustrates this shallow surface ablation on a zircon crystal face, highlighting the essentially non-destructive nature of this approach.

Determination of Growth Rates of Minerals

The capability of SIMS U–Th–Pb geochronology to provide growth rates was demonstrated using opal by Paces et al. (2004). Although Ludwig et al. (1980) recognized the ability of opal to concentrate U, making it a potential U–Pb and/or U-series chronometer, it was not until the U.S. Geological Survey started working on the Yucca Mountain project, aimed at assessing the site for a radioactive waste repository, that this potential was fully appreciated. This early work (e.g. Neymark et al. 2000) was based on TIMS analysis of U, Th and Pb chemically separated from opal samples of a few to tens of milligrams. The study demonstrated that precipitation of opal from groundwater is slow enough to result in distinguishable age differences between separate growth zones within the samples, and it highlighted the fact that the relatively large samples used in these studies contain multiple growth zones, producing a consistently discordant pattern between ^{230}Th–^{238}U ages, ^{234}U–^{238}U ages and ^{207}Pb–^{235}U ages. Furthermore, ion probe studies demonstrated that this discordance is still visible in the single-spot analyses, indicating that even these 20-micron spots produce average ages. These studies were followed by one of the few attempts to obtain high-spatial-resolution data using ID-TIMS (Paces et al. 2004).

A comparison of TIMS and SIMS data obtained for one of the opal samples from Yucca Mountain is shown in Figure 8. The sample was collected from the exploratory tunnel built to investigate the suitability of the site for the storage of radioactive waste and is similar to many other samples collected to study the hydrology of the site. It consists of 1–2 cm thick calcite and opal coatings precipitated in lithophysal cavities from water seeping through the water-unsaturated zone. Both TIMS and ion probe data show a change in the age of

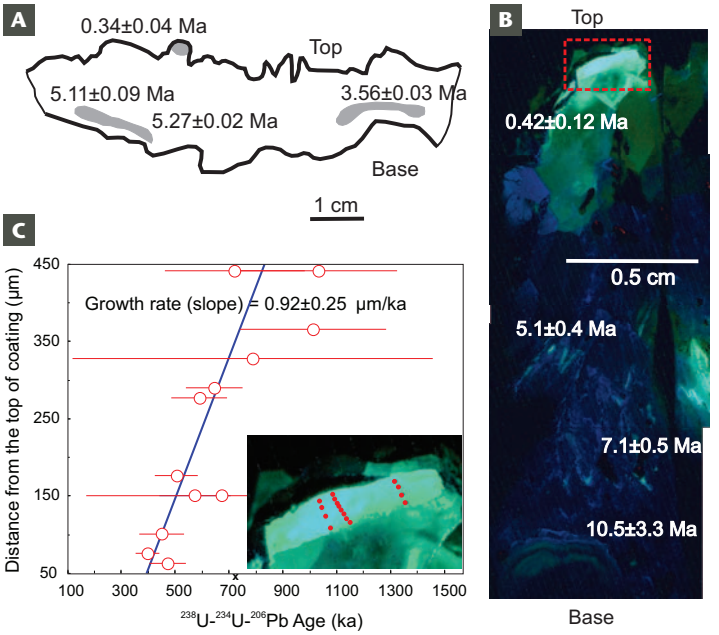

FIGURE 8 U–Pb and U-series ages of an opal sample from Yucca Mountain (Nevada, USA). (**A**) Diagram showing areas within a slice of the sample that were analysed using ID-TIMS (modified from Neymark et al. 2000). (**B**) UV-light image of different slices of the same sample analysed with SIMS, showing the ages of the investigated opal parts (dark blue is non-luminescent calcite and green is opal). (**C**) Distance versus age plot for the outermost part of the opal sample (analysed spots are shown as red dots on the insert; area of the insert is shown as a red square in (B). All errors are shown as 2σ.

the opal that is consistent with the depositional sequence from the base to the top of the coating and indicates an average deposition rate of about 2 µm/ky. The ion probe data are about an order of magnitude less precise, but the multiple analyses made along three profiles in the outermost opal layer indicate a decrease of ^{238}U–^{234}U–^{206}Pb ages consistent with the deposition order and enable an estimation of opal deposition rates close to 1 µm/ky for this layer. This rate is confirmed by the analysis of other Yucca Mountain samples (Paces et al. 2004, 2010), where the youngest-identified opal, forming hemispheres cupping calcite crystals, shows ^{238}U–^{234}U–^{230}Th and ^{238}U–^{234}U–^{206}Pb ages that suggest uninterrupted growth during the last million years, with a similar rate of about 1 µm/ky. This very slow growth of opal over the long time interval of about 10 My was used to argue for precipitation in water-unsaturated rocks above the water table and ultimately for the hydrological stability of the site and its suitability as a radioactive waste repository (Neymark et al. 2000; Paces et al. 2004, 2010). The slow opal growth also allowed a high-spatial-resolution investigation of U variations across the growth zones. These temporal U variations were found to exhibit periodicity linked to the major cycling of Earth's orbital and rotational parameters (Paces et al. 2010). As a result it is possible that opal samples worldwide preserve a record of long-term climate variations.

Sedimentary-Provenance Studies

The rapidity, access to instrumentation and facilities, and relatively low cost of analyses using high-spatial-resolution geochronological techniques have made them the dominant techniques for large-scale provenance studies. Studies of sedimentary provenance using the age spectra of detrital mineral grains (e.g. zircon, monazite and rutile) are now a key methodology in sedimentological research and commercial exploration (e.g. oil and gas and mineral deposits). Requiring the analysis of more than 100 grains per sample for statistically significant provenance results (Vermeesch 2004), a cost-effective methodology is paramount. SIMS methods have also been used to scan tens of thousands of zircon grains in Archean metasediments to identify Hadean components for studies of early Earth history (e.g. Holden et al. 2009). Such studies would not have been feasible any other way, since material consumption by laser ablation or isotope dilution techniques would have prohibited further study of these important grains.

LA–ICP–MS has found a particular niche in detrital-provenance investigations. Here the capability of recording only 30–40 seconds worth of data while achieving data uncertainties of ca. 2% (2σ) has enabled the development of this field of research. Detrital-mineral age spectra from sediment samples are used to investigate a range of problems, from local transportation mechanisms to erosion histories and regional palaeotectonic reconstructions (e.g. Alizai et al. 2011; Gehrels 2012). The rapidity of this method, while achieving uncertainty levels appropriate for the scale of the scientific question, can be used to cost-effectively provide constraints on a range of issues, from first-order questions to complex geodynamic problems, or when undertaking reconnaissance studies in remote areas with little previously acquired data or knowledge. Gehrels et al. (2008) used a data set comprising nearly 3000 analyses to illustrate differences in Himalayan strata (FIG. 9); the data indicated that the Main Central Thrust represents a major crustal divide between the two terranes involved in Himalayan orogenesis.

LA–ICP–MS also lends itself to the rapid reconnaissance of new or novel materials in geochronology (e.g. U–Pb geochronology of <1 Ma carbonates). In such cases, the elemental and isotopic variability of a material can be initially characterised, thereby allowing better understanding of formative processes and the identification of the most appropriate components for higher-precision determinations, if required. In this way, faster, lower-cost, lower-precision, high-spatial-resolution techniques (e.g. SIMS and LA–ICP–MS) can guide the cost-effective application of slower, higher-precision, lower-spatial-resolution methodologies (e.g. ID-TIMS). Used in this complementary way, the two approaches are a very powerful combination.

CONCLUSIONS

High-spatial-resolution techniques such as SIMS and LA–ICP–MS provide an essential capability in geochronology for determining age variations within mineral grains and structurally complex materials. The capability of these techniques to resolve intracrystalline heterogeneity at the micron scale – and the causative geological processes – even at lower levels of precision, renders them an essential component of the geochronologist's tool kit. The techniques enable

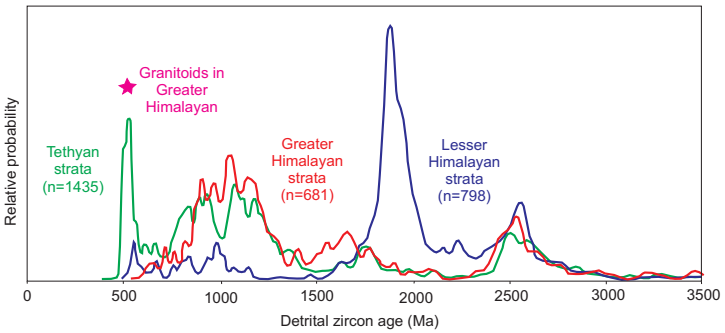

FIGURE 9 Relative age probability plot for detrital zircon data from rocks of the Nepal Himalaya (Gehrels et al. 2008). The high sample throughput possible with LA–ICP–MS lends itself well to such large-scale sedimentary provenance and erosion studies. N = number of zircon grains analysed. REPRODUCED WITH PERMISSION FROM WILEY-BLACKWELL

important scientific discovery either directly or together with higher-precision geochronological methods and other elemental and isotopic techniques. They will be key tools for geoscientists in the decades to come as the comprehension of process and effects at smaller and smaller scales becomes increasingly important.

ACKNOWLEDGMENTS

We would like to thank Axel Schmitt and John Hanchar for valuable reviews of the manuscript. We are also grateful to guest editors Daniel Condon and Mark Schmitz and principal editor John Valley for advice and suggestions, which helped to improve the paper.

REFERENCES

Alizai A, Carter A, Clift PD, VanLaningham S, Williams JC, Kumar R (2011) Sediment provenance, reworking and transport processes in the Indus River by U–Pb dating of detrital zircon grains. Global and Planetary Change 76: 33-55

Breeding CM, Ague JJ, Grove M, Rupke AL (2004) Isotopic and chemical alteration of zircon by metamorphic fluids: U–Pb age depth-profiling of zircon crystals from Barrow's garnet zone, northeast Scotland. American Mineralogist 89: 1067-1077

Cavosie AJ, Valley JW, Wilde SA, EIMF (2005) Magmatic $\delta^{18}O$ in 4400–3900 Ma detrital zircons: A record of the alteration and recycling of crust in the Early Archean. Earth and Planetary Science Letters 235: 663-681

Cavosie AJ, Valley JW, Wilde SA, EIMF (2006) Correlated microanalysis of zircon: Trace element, $\delta^{18}O$, and U–Th–Pb isotopic constraints on the igneous origin of complex >3900 Ma detrital grains. Geochimica and Cosmochimica Acta 70: 5601-5616

Cawood PA, Leitch EC, Merle RE, Nemchin AA (2011) Orogenesis without collision: Stabilizing the Terra Australis accretionary orogen, eastern Australia. Geological Society of America Bulletin 123: 2240-2255

Compston W, Pidgeon RT (1986) Jack Hills, evidence of more very old detrital zircons in Western Australia. Nature 321: 766-769

Cottle JM, Horstwood MSA, Parrish RR (2009) A new approach to single shot laser ablation analysis and its application to in situ Pb/U geochronology. Journal of Analytical Atomic Spectrometry 24: 1355-1363

Davis DW, Williams IS, Krogh TE (2003) Historical development of zircon geochronology. Reviews in Mineralogy & Geochemistry 53: 145-181

Gehrels G (2012) Detrital zircon U-Pb geochronology: Current methods and new opportunities. In: Busby C, Azor A (eds) Tectonics of Sedimentary Basins: Recent Advances. Wiley-Blackwell, Hoboken, NJ, pp 47-62

Gehrels GE, Valencia VA, Ruiz J (2008) Enhanced precision, accuracy, efficiency, and spatial resolution of U-Pb ages by laser ablation–multicollector–inductively coupled plasma–mass spectrometry. Geochemistry Geophysics Geosystems 9: Q03017, doi:10.1029/2007GC001805

Grange ML, Pidgeon RT, Nemchin AA, Timms NE, Meyer C (2013) Interpreting U–Pb data from primary and secondary features in lunar zircon. Geochimica et Cosmochimica Acta 101: 112-132

Grant ML, Wilde SA, Wu F, Yang J (2009) The application of zircon cathodoluminescence imaging, Th–U–Pb chemistry and U–Pb ages in interpreting discrete magmatic and high-grade metamorphic events in the North China Craton at the Archean/Proterozoic boundary. Chemical Geology 261: 155-171

Harrison TM, Schmitt AK, McCulloch MT, Lovera OM (2008) Early (≥4.5 Ga) formation of terrestrial crust: Lu–Hf, $\delta^{18}O$, and Ti thermometry results for Hadean zircons. Earth and Planetary Science Letters 268: 476-486

Hodges KV, Ruhl KW, Wobus CW, Pringle MS (2005) $^{40}Ar/^{39}Ar$ thermochronology of detrital minerals. Reviews in Mineralogy & Geochemistry 58: 239-257

Holden P, Lanc P, Ireland TR, Harrison TM, Foster JJ, Bruce Z (2009) Mass-spectrometric mining of Hadean zircons by automated SHRIMP multicollector and single-collector U/Pb zircon age dating: The first 100,000 grains. International Journal of Mass Spectrometry 286: 53-63

Hopkins MD, Harrison TM, Manning CE (2010) Constraints on Hadean geodynamics from mineral inclusions in >4 Ga zircons. Earth and Planetary Science Letters 298: 367-376

Kemp AIS, Whitehouse MJ, Hawkesworth CJ, Alarcon MK (2005) A zircon U-Pb study of metaluminous (I-type) granites of the Lachlan Fold Belt, southeastern Australia: implications for the high/low temperature classification and magma differentiation processes. Contributions to Mineralogy and Petrology 150: 230-249

Kemp AIS, Wilde SA, Hawkesworth CJ, Coath CD, Nemchin AA, Pidgeon RT, Vervoort JD, DuFrane SA (2010) Hadean crustal evolution revisited: New constraints from Pb–Hf isotope systematics of the Jack Hills zircons. Earth and Planetary Science Letters 296: 45-56

Kramers JD (2007) Hierarchical Earth accretion and the Hadean Eon. Journal of the Geological Society 164: 3-17

Kusiak MA, Whitehouse MJ, Wilde SA, Nemchin AA, Clark C (2013) Mobilization of radiogenic Pb in zircon revealed by ion imaging: Implications for early Earth geochronology. Geology: G33920, doi: 10.1130/G33920

Ludwig KR, Lindsey DA, Zielinski RA, Simmons KR (1980) U-Pb ages of uraniferous opals and implications for the history of beryllium, fluorine and uranium mineralization at Spor Mountain, Utah. Earth and Planetary Science Letters 46: 221-232

Nemchin A, Timms N, Pidgeon R, Geisler T, Reddy S, Meyer C (2009) Timing of crystallization of the lunar magma ocean constrained by the oldest zircon. Nature Geoscience 2: 133-136

Neymark LA, Amelin YV, Paces JB (2000) $^{206}Pb–^{230}Th–^{234}U–^{238}U$ and $^{207}Pb–^{235}U$ geochronology of Quaternary opal, Yucca Mountain, Nevada. Geochimica et Cosmochimica Acta 64: 2913-2928

Paces JB, Neymark LA, Wooden JL, Persing HM (2004) Improved spatial resolution for U-series dating of opal at Yucca Mountain, Nevada, USA, using ion-microprobe and microdigestion methods. Geochimica et Cosmochimica Acta 68: 1591-1606

Paces JB, Neymark LA, Whelan JF, Wooden JL, Lund SP, Marshall BD (2010) Limited hydrologic response to Pleistocene climate change in deep vadose zones — Yucca Mountain, Nevada. Earth and Planetary Science Letters 300: 287-298

Peck WH, Valley JW, Wilde SA, Graham CM (2001) Oxygen isotope ratios and rare earth elements in 3.3 to 4.4 Ga zircons: Ion microprobe evidence for high $\delta^{18}O$ continental crust and oceans in the Early Archean. Geochimica et Cosmochimica Acta 65: 4215-4299

Pidgeon RT, Nemchin AA (2006) High abundance of early Archean grains and the age distribution of detrital zircons in a sillimanite-bearing quartzite from Mt Narryer, Western Australia. Precambrian Research 150: 201-220

Rasmussen B, Fletcher IR, Muhling JR (2011a) Response of xenotime to prograde metamorphism. Contributions to Mineralogy and Petrology 162: 1259-1277

Rasmussen B, Fletcher IR, Muhling JR, Gregory CJ, Wilde SA (2011b) Metamorphic replacement of mineral inclusions in detrital zircon from Jack Hills, Australia: Implications for the Hadean Earth. Geology 39: 1143-1146

Scherer EE, Whitehouse MJ, Münker C (2007) Zircon as a monitor of crustal growth. Elements 3: 19-24

Tatsumoto M, Premo WR, Unruh DM (1987) Origin of lead from green glass of Apollo 15426: A search for primitive lunar lead. Journal of Geophysical Research 92: E361-E371

Vermeesch P (2004) How many grains are needed for a provenance study? Earth and Planetary Science Letters 224: 441-451

Watson EB, Harrison TM (2005) Zircon thermometer reveals minimum melting conditions on earliest Earth. Science 308: 841-844

BRUKER

µm-cm 3D Chemical Analysis

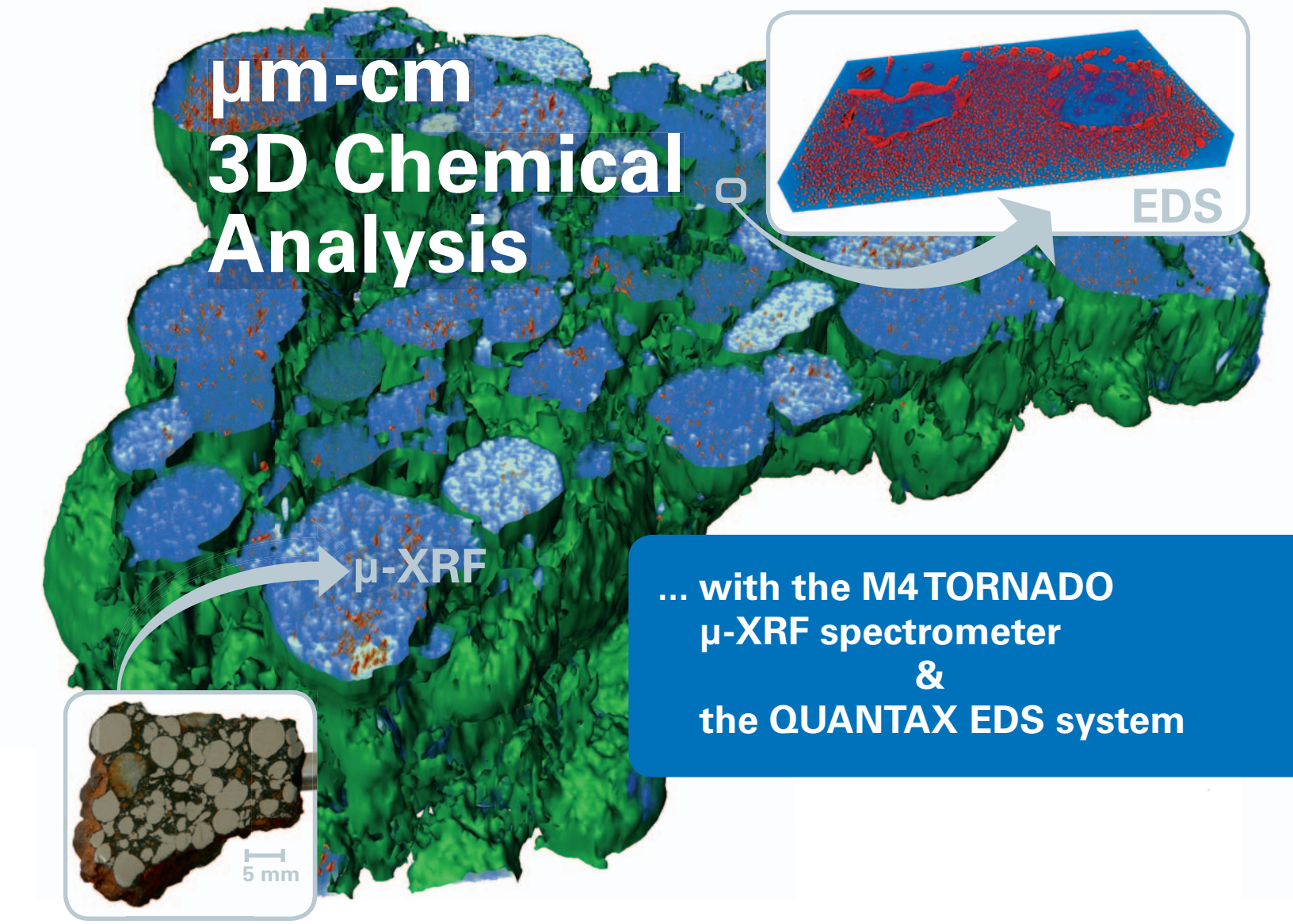

... with the M4 TORNADO µ-XRF spectrometer & the QUANTAX EDS system

Analyze up to 12 orders of magnitude larger samples without longer measuring times using µ-XRF and SEM/EDS with serial sectioning instead of 3D EDS focused ion beam (FIB) analysis!
The Gujba meteorite sample shown above was mapped with a M4 TORNADO µ-XRF spectrometer (36 2D-sections). The 3D reconstruction of the µ-XRF data (voxel size: 32x32x148 µm) shows the surfaces of Fe,Ni-metal particles in green and sulfides in red. The Ni-content of the metal particles varies from 5 wt% (dark blue) to 8 wt% (light blue). A smaller area was mapped with a QUANTAX EDS system (21 2D-sections). The 3D reconstruction of the EDS data (voxel size:1.6x1.6x4 µm) shows Fe (blue) and S (red).

More details can be found at: www.bruker.com/elements